*To be published in Optics Letters:*

**Title:** Electrically-pumped continuous-wave O-band quantum-dot superluminescent diode on silicon

**Authors:** ying lu,Victoria Cao,Mengya liao,Wei Li,Mingchu Tang,Ang Li,Peter Smowton,Alwyn Seeds,Huiyun Liu,Siming Chen

**Accepted:** 03 August 20

**Posted** 03 August 20

**DOI:** https://doi.org/10.1364/OL.401042

# Electrically-pumped continuous-wave O-band quantum-dot superluminescent diode on silicon

YING LU,[1,†] VICTORIA CAO,[1,†] MENGYA LIAO,[1,4] WEI LI,[2] MINGCHU TANG,[1] ANG LI,[2] PETER SMOWTON,[3] ALWYN SEEDS,[1] HUIYUN LIU,[1] AND SIMING CHEN[1,*]

[1]Department of Electronic and Electrical Engineering, University College London, Torrington Place, London WC1E 7JE, UK
[2]Institute of Microstructure and Properties of Advanced Materials, Beijing University of Technology, Beijing 100124, China
[3]Department of Physics and Astronomy, Cardiff University, Queens Building, The Parade, Cardiff CF24 3AA, UK
[4]e-mail: mengya.liao@ucl.ac.uk
*Corresponding author: siming.chen@ucl.ac.uk

Received XX Month XXXX; revised XX Month, XXXX; accepted XX Month XXXX; posted XX Month XXXX (Doc. ID XXXXX); published XX Month XXXX

**High-power, broadband quantum dot (QD) superluminescent diodes (SLDs) are ideal light sources for optical coherence tomography (OCT) imaging systems but have previously mainly been fabricated on native GaAs- or InP-based substrates. Recently, significant progress has been made to emigrate QD SLDs from native substrates to silicon substrates. Here, we demonstrate electrically pumped continuous-wave (CW) InAs QD SLDs monolithically grown on silicon substrates with significantly improved performance thanks to the achievement of a low density of defects in the III-V epilayers. The fabricated narrow ridge-waveguide device exhibits a maximum 3-dB bandwidth of 103 nm emission spectrum centred at O-band together with a maximum single-facet output power of 3.8 mW at room temperature. The silicon based SLD has been assessed for application in an OCT system. Under optimised conditions, a predicted axial resolution of ~ 5.3 µm is achieved with a corresponding output power of 0.66 mW/facet. The realisation of high-performance III-V SLDs on silicon substrates will be the enabling technology for low-cost, large-scale deployment of fully integrated silicon photonic OCT systems.** 

http://dx.doi.org/10.1364/OL.99.099999

Silicon photonics has been under intensive development over the past decade and is reaching the tipping point. While such technology for data- and tele-communications applications is well known and attracting great interest [1], its potential for other applications, for example, medical diagnostics [2], chemical and biological sensing [3], and nonlinear optics [4], is now building on this progress by leveraging the greatest promise of silicon photonics: large-scale, streamlined manufacturing using commercial CMOS foundry infrastructure. Optical coherence tomography (OCT) has become a powerful medical diagnostic tool to monitor medical treatment and diagnose disease within the skin and other biological tissues non-invasively [5]. The technique currently relies on costly and bulky combinations of separate light source, optical and electronic components. As a result, there is a strong motivation to achieve a low-cost, compact, and maintenance-free biomedical imaging solution using CMOS-compatible photonic integrated circuits (PICs), which could potentially allow monolithic integration of low-loss silicon/SiNx waveguides, high-speed silicon photodiodes and electronics combined with the hetero-integration of an efficient and reliable III-V- or, in a longer term, simply silicon-based [6,7] light source. Various demonstrations have shown the potential of silicon photonic integrated chips for OCT [8-10], yet, all have required external III-V light sources. This limits the potential for ultra-compact and large-scale integration. The availability of integrated light sources is, therefore, a key technology for a fully integrated silicon photonic OCT system.

OCT is based upon low-coherence interferometry [11], in doing so, broadband light sources, rather than coherent laser sources, are required. Superluminescent diodes (SLDs), offering both low-coherence and high output power, permit a low-cost and robust route to provide high axial resolution and deep penetration in such scenarios [12]. Self-assembled quantum dots (QDs) constructed by the Stranski-Krastanov growth method have been extensively studied for SLDs over the past two decades, with a view to achieving a broad bandwidth enabled by their naturally occurring large size inhomogeneity, which could also be extended by using of both the ground and excited states for even broader emission [13]. Recently, the self-assembled QD technique is gaining even more importance due to the emergence of promising monolithic III-V/silicon photonic integration applications. Their unique properties, in particular, the enhanced tolerance to defects [14] and reflections [15], as well as the ultralow linewidth enhancement factor [16], have witnessed rapid development in various types of O-band InAs/GaAs QD lasers grown directly on silicon substrates [17-25]. Despite significant progress being made in QD lasers grown

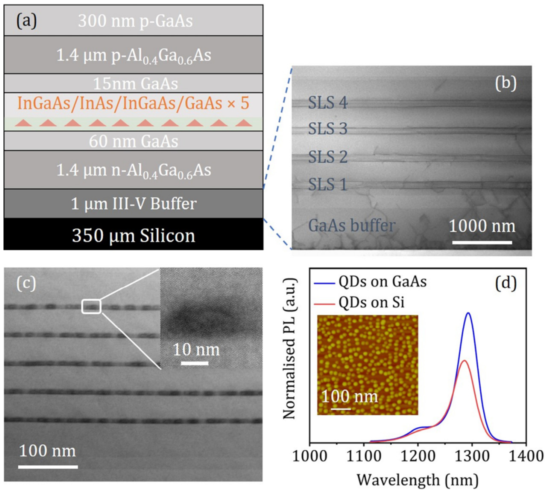


Fig. 1. (a) Schematic layer structure of the InAs QD SLD on silicon. (b) Bright-field scanning TEM image of an III-V buffer layer grown on silicon. (c) Bright-field scanning TEM image of the QD active layers. The inset shows the high-resolution bright-field scanning TEM image of a single dot. (d) PL comparison of InAs/GaAs QDs SLD structure grown on silicon to a reference sample grown on native GaAs under the same excitation conditions. The inset shows the representative AFM image of an uncapped QD sample grown on silicon.

on silicon substrates and QD SLDs on native GaAs substrates [26-30], respectively, a high power, broadband continuous-wave (CW) InAs QD SLD monolithically grown on a silicon substrate has not yet been demonstrated as a result of the massive material dissimilarity between the two material systems [31].

We have previously demonstrated the first electrically pumped monolithic SLD on silicon by using GaAs nucleation layer (NL), and InAlAs/GaAs strained layer superlattices (SLSs) combined with InAs QDs act as the active region [32]. However, the devices are limited to pulsed operation. While the first successful demonstration of a CW silicon based InAs QDs SLD followed soon after [33], these CW devices showed significantly diminished performance in terms of maximum achievable emission bandwidth (~50 nm) and output power (~0.55 mW) mainly because of material quality issues and imperfect device fabrication. Very recent advanced epitaxial techniques for III-V buffer layers have enabled dramatically reduced threading dislocation density from ~ $10^8$ $cm^{-2}$ to ~ $10^6$ $cm^{-2}$ [17]. Building on this foundation, in this work, we demonstrate high-performance electrically pumped CW O-band InAs/GaAs QD SLDs monolithically grown on silicon substrates. The anti-reflection (AR) coating-free ridge-waveguide device achieved CW single facet output power over 3.8 mW at room temperature (RT); The balanced amplified spontaneous emission (ASE) from both ground and excited states enabled a maximum emission bandwidth of > 100 nm, centered at ~1272 nm, corresponding to a minimum axial resolution of 5.3 μm, offering the possibility to perform next-generation silicon photonic OCT for imaging skin tissues.

Figure 1(a) illustrates the schematic of the whole separate confinement heterostructure on a silicon substrate. In this work, the n-doped silicon (001) wafer with a 4° miscut towards the [011] plane was used to suppress the formation of antiphase domains (APDs), and the InAs QDs structures were directly grown on this silicon wafer by using solid-source molecular

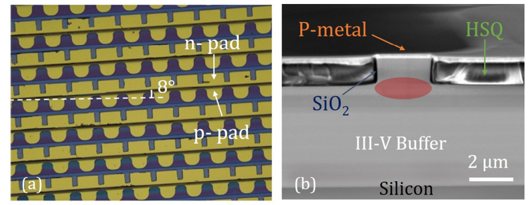


Fig. 2. (a) An optical micrography of rows of fabricated narrow-ridge waveguide SLDs. (b) A cross-sectional SEM image of the fabricated SLD with as-cleaved facets.

beam epitaxy. The deoxidisation process of the silicon substrate was firstly implemented in the MBE chamber at 900°C for 20 mins. Epitaxy was then performed in the following order: a III-V buffer layer, consisting of a 6 nm AlAs NL grown at 350 °C, a 1 μm GaAs buffer layer using a three-step growth technique and 4 layers of InGaAs/GaAs SLSs combined with *in situ* thermal annealing [17], an n-type $Al_{0.4}Ga_{0.6}As$ in a thickness of 1400 nm, which acts as the lower cladding layer, a 60 nm GaAs lower waveguide layer, a five-layer of InAs/GaAs dot-in-a-well (DWELL) active region, a 60 nm GaAs upper waveguide layer, a 1400 nm p-type $Al_{0.4}Ga_{0.6}As$ upper cladding layer, and finally a 300 nm highly p-doped GaAs contact layer. Each DWELL structure consisted of a 3-monolayer layer of InAs QDs sandwiched by 2 nm $In_{0.15}Ga_{0.85}As$ and 6 nm $In_{0.15}Ga_{0.85}As$ and separated by 45 nm undoped GaAs spacer layers. The DWELLs were grown at 510 °C, and GaAs and AlGaAs layers were grown at 590 °C.

Figure 1(b) presents a bright-field scanning transmission electron microscopy (BF-STEM) image of the III-V buffer layer grown on a silicon substrate. As expected, a high density of dislocations is generated at the III-V/silicon interface due to the large lattice mismatch between III-V and silicon. Fortunately, it is clear to see that, after the last set of InGaAs/GaAs SLSs, most of the defects have been filtered. Above all, a nearly defect-free DWELL active region is observed as seen in Fig. 1(c). Figure 1(d) compares the photoluminescence (PL) emission of QDs grown on silicon and GaAs substrates, where a comparable PL intensity of QDs on silicon to that of on GaAs is obtained. The slight blueshift in the peak emission wavelength is mainly attributed to the residual strain between GaAs and silicon. These findings suggest that the III-V buffer layer plays a critical role in suppressing the formation of APBs, and the propagation of threading dislocations, thanks to the combined strategies of an AlAs NL, InGaAs/GaAs SLSs, and *in situ* thermal annealing. The inset of Fig. 1(c) shows the atomic-resolution BF-STEM image of a single dot, where the typical dot size is ~20 nm in diameter and ~7 nm in height. The inset of Fig. 1d shows an atomic force microscopy (AFM) image for uncapped InAs QDs grown on silicon. An average dot density of ~$3\times10^{10}$ $cm^{-2}$ was derived from the image. A maximum net modal gain of ~ 13 $cm^{-1}$ at the ground state (GS) peak wavelength was obtained in this structure by a segmented-contact method.

Optical microscopy and scanning electron microscopy (SEM) images of the fabricated devices are shown in Fig. 2. The 2.2 μm width ridge waveguides were defined using electron beam lithography (EBL) and dry etching. To avoid oxidation of the Al-containing layers, a passivation layer of $SiO_2$ was first deposited. Planarisation was then carried out by using hydrogen silsesquioxane (HSQ) thermally cured at 180 °C. For the ohmic contact metallisation, Ti/Pt/Au and Au/GeAu/Ni/Au were used for the P+ GaAs contacting layer and the exposed n+ GaAs layer,

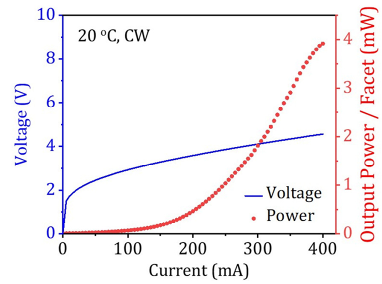


Fig. 3. *LIV* characteristics of a 2.2 µm × 4 mm InAs/GaAs QD SLD grown on a silicon substrate under CW operation.

respectively. The device cavity length for all devices described in this letter is 4 mm and is defined by cleaving. No facet coating is applied. To achieve only ASE, the device was protected against the laser effect by suppressing cavity reflections using an 8° off-angle tilted waveguide. The SLD bars were mounted epi-side up on a copper heat sink using indium silver low-melting-point solder and directly probed to enable testing. Unless stated otherwise, all SLD measurements were performed under CW operation at RT (20 °C) with no active cooling.

Figure 3 shows the light-current-voltage (*LIV*) measurement for a typical InAs/GaAs QD SLD grown on a silicon substrate. As seen, above a current of ~100 mA, an apparent superluminescent behaviour is evidenced by the superlinear increase in output power with increasing current. A single facet output power of 3.8 mW was obtained at an injection current of 400 mA, with only slight power roll over at this current due to the thermal effects. For application in OCT systems, higher power is desired for better depth penetration. As the output power spectrum depends linearly on spontaneous emission rate and exponentially on the optical gain, it follows that a high value of modal gain is critical for obtaining high output power.

In addition to output power, another critical factor for high-quality OCT images is the spectral bandwidth, since the axial resolution is governed by the coherence length, which is inversely proportional to the spectral bandwidth of the light source deployed in the system. Figure 4 shows the ASE spectra and, correspondingly, the evolution of the 3-dB linewidth as well as the central wavelength as a function of injection current. At a low drive current of 40 mA, the emission is dominated by the GS of the QDs centred at 1310 nm, with a 3-dB bandwidth of ~ 47.3 nm. At higher currents, the GS peak intensity saturates, and the spectra are broadened sharply to higher energies (shorter wavelengths) due to the sequential carrier filling of the QD's first excited state (ES1). At a current of 200 mA, the ASE from GS and ES1 is well balanced, giving rise to a maximum 3-dB bandwidth of 103 nm. With the further increase of the current over 200 mA, the emission spectrum becomes dominated by the ES1 leading to a significant reduction in the 3-dB linewidth.

To gain further insight into the interplay of bandwidth and central wavelength of the emission spectrum on the axial resolution in OCT, this silicon based QD SLD is assessed theoretically through the self-coherence function under different operating conditions. This self-coherence function is calculated by the inverse Fourier transform of the power spectral density (PSD) of the SLD, in analogy to the point spread function (PSF) of the imaging system [34]. By assuming the emission to be Gaussian, the axial resolution would be half of the full-width-at-half-maximum (FHWM) of the coherence length.

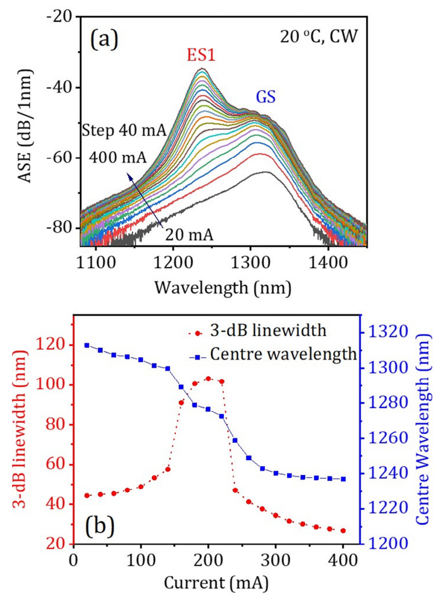


Fig. 4. (a) Spectrally resolved in-fiber ASE power as a function of injection current. (b) Evolution of the 3-dB bandwidth and the center wavelength against the injection current.

Figure 5(a) depicts an example of self-coherence function derived from the ASE spectrum (shown in the inset of Fig. 5(a)) where the 3-dB bandwidth of 103 nm centred at 1276 nm. A minimum axial resolution of 5.2 µm is predicted. Undesirable sidelobes are observed due to the non-Gaussian ASE spectrum; this introduces a penalty to axial resolution and could be minimised by reducing the ASE spectrum dips between the GS and ES1. Figure 5(b) shows the dependence of predicted axial resolution and measured single facet output power on the injection current. As seen, while a minimum predicted axial resolution of 5.2 µm was achieved at 200 mA, the corresponding output power was less than 0.5 mW. With the increase of the current above 200 mA, there is a trade-off between the axial resolution and output power. As a result, at 400 mA, although a high single facet output power of 3.8 mW was obtained, the predicted axial resolution has been significantly reduced to 18.9 µm. Under the optimised condition of 220 mA, a good axial resolution of 5.3 µm was realised with a reasonable corresponding output power of 0.66 mW.

Although QD SLD presented in this work demonstrated much superior performance over previous works on monolithic III-V SLDs on silicon, their device performance is inferior when compared to native GaAs substrates previously reported in terms of output power and spectrum bandwidth. Output power can be increased in future devices by increasing the overall dot density through high-density QD growth combined with its multilayer growth [35] and the use of p-type modulation doping of the active region [36]. Strategies to further improve the spectral bandwidth are multifaceted: chirped QDs [37], QD intermixing [38], and hybrid quantum well / QD structures [39].

In summary, we have demonstrated a RT electrically pumped CW InAs/GaAs QD SLD directly grown on a silicon substrate with significantly improved CW performance compared to previous reports. The high-quality III-V epilayers and the use of InAs QDs as the active region lead to a maximum 3-dB linewidth of 103 nm centred at 1275 nm together with a maximum single facet output power over 3.8 mW from a narrow-ridge tilted waveguide AR-coating free device. Assessment of this silicon

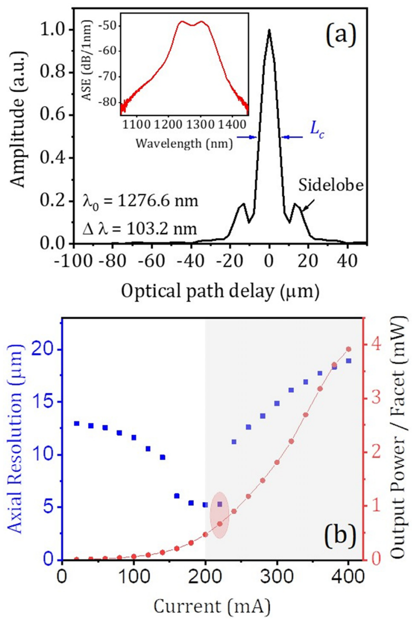


Fig. 5. (a) Self-coherence function calculated from emission spectrum shown in the inset of Fig.5(a). (b) Dependence of predicted axial resolution and single facet output power on the injection current.

based SLD for OCT application indicates that an axial resolution of 5.3 μm should be possible with a corresponding single facet output power of 0.66 mW. The successful demonstration of high-performance QD SLDs on silicon substrates opens the way for exploiting low-cost, miniaturised OCT for medical diagnosis.

**Funding.** Royal Academy of Engineering (RAEng) (RF201617/16/28); Engineering and Physical Sciences Research Council (EPRSRC) (EP/T01394X/1); Beijing Natural Science Foundation (No. Z180014).

**Acknowledgement**. YL and VC thank EPSRC for funding their PhD studies. SC thanks the Royal Academy of Engineering (RAEng) for funding his Research Fellowship.

**Disclosures**. The authors declare no conflicts of interest.

## REFERENCES

1. D. Liang and J. E. Bowers, Nat. Photon. **4**, 517 (2010).
2. A. L. Washburn, L. C. Gunn, and R. C. Bailey, Anal. Chem. **81**, 9499 (2009).
3. K. Xu, Y. Chen, T. Okhai, and L.. Snyman, Opt. Mater. Express **9**, 3985 (2019).
4. J. Leuthold, C. Koos, and W. Fredue, Nat. Photon. **4**, 535 (2010).
5. W. Drexler and J. G. Fujimoto, Berlin, Germany/New York: Spring-Verlag, (2008).
6. Y. Chen, D. Xu, K. Xu, N. Zhang, S. Liu, J. Zhao, Q. Luo, L. W. Snyman, and J. W. Swart, Chin. Phys. B **28**, 107801 (2019).
7. K. Xu, Phys. Status Solidi A **216**, 1800868 (2019).
8. G. Yurtsever, N. Weiss, J. Kalkman, T. G. van Leeuwen, and R. Baets, Opt. Lett. **39**, 5228 (2014).
9. Z. Wang, H.-C. Lee, D. Vermeulen, L. Chen, T. Nielsen, S. Y. Park, A. Ghaemi, E. Swanson, C. Doerr, and J. Fujimoto, Biomed. Opt. Express **6**, 2562 (2015).
10. S. Schneider, M. Lauermann, P-I. Dietrich, C. Weimann, W. Freude, and C. Koos, Opt. Lett. **24**, 1573 (2016).
11. D. Huang, E. A. Swanson, C. P. Lin, J. S. Schuman, W. G. Stinson, W. Chang, M. R. Hee, T. Flotte, K. Gregory, C. A. Puliafito, and J. G. Fujimoto, Science **254**, 1178 (1991).
12. T. H. Ko, D. C. Adler, J. G. Fujimoto, D. Mamedov, V. Prokhorov, V. Shidlovski, and S. Yakubovich, Opt. Express **12**, 2112 (2004).
13. Z. Zhang, R. A. Hogg, X. Lv, Z. Wang, Adv. Opt. Photon. **2**, 201 (2010).
14. Z. Liu, C. Hantschmann, M. Tang, Y. Lu, J-S. Park, M. Liao, S. Pan, A. M. Sanchez, R. Beanland, M. Martin, T. Baron, S. Chen, A. Seeds, I. White, R. Penty, H. Liu, J. Lightw. Technol. **38**, 240 (2020).
15. H. Huang, J. Duan, B. Dong, J. Norman, D. Jung, J. E. Bowers, and F. Grillot, APL Photon. **5**, 016103 (2020).
16. J. Duan, H. Huang, D. Jung, Z. Zhang, J. Norman, J. E. Bowers, and F. Grillot, Appl. Phys. Lett. **112**, 251111 (2018).
17. S. Chen, W. Li, J. Wu, Q. Jiang, M. Tang, S. Shutts, S. N. Elliott, A. Sobiesierski, A. J. Seeds, I. Ross, P. M. Smowton, and H. Liu, Nat. Photon. **10**, 307 (2016).
18. M. Liao, S. Chen, Z. Liu, Y. Wang, L. Ponnampalam, Z. Zhou, J. Wu, M. Tang, S. Shutts, Z. Liu, P. M Smowton, S. Yu, A. Seeds, and H. Liu, Photonics Res. **6**, 1062 (2018).
19. Y. Wang, S. Chen, Y. Yu, L. Zhou, L. Liu, C. Yang, M. Liao, M. Tang, Z. Liu, J. Wu, W. Li, I. Ross, A. Seeds, H. Liu, S. Yu, Optica **5**, 528 (2018).
20. W. Q. Wei, J. H. Wang, B. Zhang, J. Y. Zhang, H. L. Wang, Q. Feng, H. X. Xu, T. Wang, and J. J. Zhang, Appl. Phys. Lett. **113**, 053107 (2018).
21. S. Liu, X. Wu, D. Jung, J. C. Norman, M. J. Kennedy, H. K. Tsang, A. C. Gossard, and J. E. Bowers, Optica **6**, 128 (2019).
22. Y. Wan, S. Zhang, J. C. Norman, M. J. Kennedy, W. He, S. Liu, C. Xiang, C. Shang, J. He, A. C. Gossard, and J. E. Bowers, Optica **6**, 1394 (2019).
23. W. Q. Wei, J. Y. Zhang, J. H. Wang, H. Cong, J. J. Guo, Z. H. Wang, H. X. Xu, T. Wang and J. J. Zhang, Opt. Lett. **45**, 2042 (2020)
24. T. Zhou, M. Tang, G. Xiang, B. Xiang, S. Hark, M. Martin, T. Baron, S. Pan, J-S. Park, Z. Liu, S. Chen, Z. Zhang and H. Liu, Nat. Commun. **11**, 977 (2020).
25. Y. Wan, J. C. Norman, Y. Tong, M. J. Kennedy, W. He, C. Shang, M. Dumont , A. Malik, H. K. Tsang, A. C. Gossard, J. E. Bowers, Laser Photonics Rev. **14**, 2000037 (2020).
26. S. Chen, W. Li, Z. Zhang, D. Childs, K. Zhou, J. Orchard, K. Kennedy, M. Hugues, E. Clarke, I. Ross, O. Wada and R. Hogg, Nanoscale Res. Lett. **10**, 340 (2016).
27. C. Hou, H. Chen, J. Zhang, N. Zhuo, Y. Huang, R. Hogg, D. Childs, J. Ning, Z. Wang, F. Liu and Z. Zhang, Light Sci. Appl. **7**, 17170 (2018).
28. N. Ozaki, D. T. D. Childs, J. Sarma, T. S. Roberts, T. Yasuda, H. Shibata, H. Ohsato, E. Watanabe, N. Ikeda, Y. Sugimoto, and R. A. Hogg, J Appl. Phys. **119**, 083107 (2016).
29. A. F. Forrest, M. Krakowski, P. Bardella, and M. A. Cataluna, Opt. Express **27**, 10981 (2019).
30. N. Ozaki, S. Yamauchi, Y. Hayashi, E. Watanabe, H. Ohsato, N. Ikeda, Y. Sugimoto, K. Furuki, Y. Oikawa and K. Miyaji, D. T D Childs and R. A. Hogg, J. Appl. Phys D: Appl Phys, **52**, (2019).
31. M. Liao, S. Chen, J-S. Park, A. Seeds, H. Liu, Semicond. Sci. Technol. **33**, 123002 (2018).
32. S. Chen, M. Tang, Q. Jiang, J. Wu, V. Dorogan, M. Benamara, Y. Mazur, G. Salamo, P. Smowton, A. Seeds, and H. Liu, ACS Photon. **1**, 638 (2014).
33. M. Liao, S. Chen, S. Huo, S. Chen, J. Wu, M. Tang, K. Kennedy, W. Li, S. Kumar, M. Martin, T. Baron, C. Jin, I. Ross, A. Seeds and H. Liu, IEEE J. Sel. Top. Quantum Electron. **23**, 1900910 (2017).
34. C. Akay, P. Parrein, and J. Rolland, Appl. Opt. **41**, 5256 (2002).
35. K. Nishi, K. Takemasa, and M. Sugawara, IEEE J. Sel. Topics Quantum Electron. **23**, 1901007 (2017).
36. M. Sugawara and M. Usami, Nat. Photon. **3**, 30 (2009).
37. L. Li, M. Rossetti, A. Fiore, L. Occhi, and C. Velez, Electron. Lett. **41**, 41 (2005).
38. K. Zhou, Q. Jiang, Z. Zhang, S. Chen, H. Liu, Z. Lu, K. Kennedy, S. Matcher, R. Hogg, Opt. Express, **20**, 26950 (2012).
39. S. Chen, K. Zhou, Z. Zhang, D. T. D. Childs, M. Hugues, A. J. Ramsay, and R. A. Hogg, Appl. Phys. Lett. **100**, 041118 (2012).

## REFERENCES


1. D. Liang and J. E. Bowers, Recent progress in lasers on silicon, Nat. Photon. **4**, 511-517 (2010)
2. A. L. Washburn, L. C. Gunn, and R. C. Bailey, Label-Free Quantitation of a Cancer Biomarker in Complex Media Using Silicon Photonic Microring Resonators, Anal. Chem. **81**, 9499 (2009).
3. K. Xu, Y. Chen, T. A. Okhai, and L. W. Snyman, Micro optical sensors based on avalanching silicon light-emitting devices monolithically integrated on chips, Opt. Mater. Express **9**, 3985 (2019).
4. J. Leuthold, C. Koos, and W. Fredue, Nonlinear silicon photonics, Nat. Photon. **4**, 535 (2010).
5. W. Drexler and J. Fujimoto, Optical Coherence Tomography: Technology and Applications. Berlin, Germany/New York: Spring-Verlag, 2008.
6. Y. Chen, D. Xu, K. Xu, N. Zhang, S. Liu, J. Zhao, Q. Luo, L. W. Snyman, and J. W. Swart, Optoelectronic properties analysis of silicon light-emitting diode monolithically integrated in standard CMOS IC, Chin. Phys. B **28**, 107801 (2019).
7. K. Xu, Silicon MOS Optoelectronic Micro-Nano Structure Based on Reverse-Biased PN Junction, Phys. Status Solidi A **216**, 1800868 (2019).
8. G. Yurtsever, N. Weiss, J. Kalkman, T. G. van Leeuwen, and R. Baets, Ultra-compact silicon photonic integrated interferometer for swept-source optical coherence tomography, Opt. Lett. **39**, 5228 (2014).
9. Z. Wang, H.-C. Lee, D. Vermeulen, L. Chen, T. Nielsen, S. Park, A. Ghaemi, E. Swanson, C. Doerr, and J. Fujimoto, Silicon photonic integrated circuit swept-source optical coherence tomography receiver with dual polarisation, dual balanced, in-phase and quadrature detection, Biomed. Opt. Express **6**, 2562 (2015).
10. S. Schneider, M. Lauermann, P-I. Dietrich, C. Weimann, W. Freude, and C. Koos, Optical coherence tomography system mass-producible on a silicon photonic chip, Opt. Lett. **24**, 1573 (2016).
11. D. Huang, E. A. Swanson, C. P. Lin, J. S. Schuman, W. G. Stinson, W. Chang, M. R. Hee, T. Flotte, K. Gregory, C. A. Puliafito, and J. G. Fujimoto, Optical coherence tomography, Science **254**, 1178 (1991).
12. T. Ko, D. Adler, J. Fujimoto, D. Mamedov, V. Prokhorov, V. Shidlovski, and S. Yakubovich, Ultrahigh resolution optical coherence tomography imaging with a broadband superluminescent diode light source, Opt. Express **12**, 2112 (2004)
13. Z. Zhang, R. Hogg, X. Lv, Z. Wang, Self-assembled quantum-dot superluminescent light-emitting diodes. Adv. Opt. Photonics **2**, 201 (2010)
14. Z. Liu, C. Hantschmann, M. Tang, Y. Lu, J-S. Park, M. Liao, S. Pan, A. Sanchez, R. Beanland, M. Martin, T. Baron, S. Chen, A. Seeds, I. White, R. Penty, H. Liu, Origin of Defect Tolerance in InAs/GaAs Quantum Dot Lasers Grown on Silicon, J. Lightw. Technol. **38**, 240 (2020).
15. H. Huang, J. Duan, B. Dong, J. Norman, D. Jung, J. E. Bowers, and F. Grillot, Epitaxial quantum dot lasers on silicon with high thermal stability and strong resistance to optical feedback, APL Photon. **5**, 016103 (2020).
16. J. Duan, H. Huang, D. Jung, Z. Zhang, J. Norman, J. Bowers, and F. Grillot, Semiconductor quantum dot lasers epitaxially grown on silicon with low linewidth enhancement factor, Appl. Phys. Lett. **112**, 251111 (2018).
17. S. Chen, W. Li, J. Wu, Q. Jiang, M. Tang, S. Shutts, S. N. Elliott, A. Sobiesierski, A. J. Seeds, I. Ross, P. M. Smowton, and H. Liu, Electrically pumped continuous-wave III-V quantum dot lasers on silicon, Nat. Photonics **10**, 307 (2016).
18. M. Liao, S. Chen, Z. Liu, Y. Wang, L. Ponnampalam, Z. Zhou, J. Wu, M. Tang, S. Shutts, Z. Liu, P. Smowton, S. Yu, A. Seeds, and H. Liu, Low-Noise 1.3 µm InAs/GaAs Quantum Dot, Photonics Res. 6, 1062 (2018).
19. Y. Wang, S. Chen, Y. Yu, L. Zhou, L. Liu, C. Yang, M. Liao, M. Tang, Z. Liu, J. Wu, W. Li, I. Ross, A. Seeds, H. Liu, S. Yu, Monolithic quantum-dot distributed feedback laser array on silicon, Optica **5**, 528 (2018).
20. W. Wei, J. Wang, B. Zhang, J. Zhang, H. Wang, Q. Feng, H. Xu, T. Wang, and J. Zhang, "InAs QDs on (111)-faceted Si (001) hollow substrates with strong emission at 1300 nm and 1550 nm," Appl. Phys. Lett. **113**, 053107 (2018).
21. S. Liu, X. Wu, D. Jung, J. C. Norman, M. J. Kennedy, H. Tsang, A. Gossard, and J. Bowers, High-channel-count 20 GHz passively mode-locked quantum dot laser directly grown on Si with 4.1 Tbit/s transmission capacity, Optica **6**, 128 (2019).
22. Y. Wan, S. Zhang, J. Norman, M. Kennedy, W. He, S. Liu, C. Xiang, C. Shang, J. He, A. Gossard, and J. Bowers, Tunable quantum dot lasers grown directly on silicon, Optica **6**, 1394 (2019).
23. W. Wei, J. Zhang, J. Wang, H. Cong, J. Guo, Z. Wang, H. Xu, T. Wang and J. Zhang, "Phosphorus-free 1.5 µm InAs quantum-dot microdisk lasers on metamorphic InGaAs/SOI platform," Opt. Lett. **45**, 2042 (2020)
24. T. Zhou, M. Tang, G. Xiang, B. Xiang, S. Hark, M. Martin, T. Baron, S. Pan, J-S. Park, Z. Liu, S. Chen, Z. Zhang and H. Liu, Continuous-wave quantum dot photonic crystal lasers grown on on-axis Si (001). Nat. Commun. **11,** 977 (2020).
25. Y. Wan, J. Norman, Y. Tong, M. Kennedy, W. He, C. Shang, M. Dumont , A. Malik, H. Tsang, A. Gossard, J. Bowers, 1.3 µm Quantum Dot-Distributed Feedback Lasers Directly Grown on (001) Si, Laser Photonics Rev. **14**, 2000037 (2020).
26. S. Chen, W. Li, Z. Zhang, D. Childs, K. Zhou, J. Orchard, K. Kennedy, M. Hugues, E. Clarke, I. Ross, O. Wada and R. Hogg, GaAs-based superluminescent light-emitting diodes with 290-nm emission bandwidth by using hybrid quantum well/quantum dot structures， Nanoscale Res. Lett. 10, 340 (2015).
27. C. Hou, H. Chen, J. Zhang, N. Zhuo, Y. Huang, R. Hogg, D. Childs, J. Ning, Z. Wang, F. Liu and Z. Zhang, Near-infrared and mid-infrared semiconductor broadband light emitters. Light Sci. Appl. **7,** 17170 (2018).
28. N. Ozaki, D. Childs, J. Sarma, T. Roberts, T. Yasuda, H. Shibata, H. Ohsato, E. Watanabe, N. Ikeda, Y. Sugimoto, and R. Hogg, Superluminescent diode with a broadband gain based on self-assembled InAs quantum dots and segmented contacts for an optical coherence tomography light source, J Appl. Phys. **119**, 083107 (2016).
29. A. F. Forrest, M. Krakowski, P. Bardella, and M. A. Cataluna, High-power quantum-dot superluminescent tapered diode under CW operation, Opt. Express **27**, 10981 (2019).
30. N. Ozaki, S. Yamauchi, Y. Hayashi, E. Watanabe, H. Ohsato, N. Ikeda, Y. Sugimoto, K. Furuki, Y. Oikawa and K. Miyaji, D. Childs and R. Hogg, Development of a broadband superluminescent diode based on self-assembled InAs quantum dots and demonstration of high-axial-resolution optical coherence tomography imaging, J. Appl. Phys D: Appl Phys, **52**, (2019).
31. M. Liao, S. Chen, J-S. Park, A. Seeds, H. Liu, III–V quantum-dot lasers monolithically grown on silicon, Semicond. Sci. Technol. **33,** 123002 (2018).
32. S. Chen, M. Tang, Q. Jiang, J. Wu, V. Dorogan, M. Benamara, Y. Mazur, G. J. Salamo, P. Smowton, A. Seeds, and H. Liu, InAs/GaAs Quantum-Dot Superluminescent Light-Emitting Diode Monolithically Grown on a Si Substrate, ACS Photonics **1**, 638 (2014).
33. M. Liao, S. Chen, S. Huo, S. Chen, J. Wu, M. Tang, K. Kennedy, W. Li, S. Kumar, M. Martin, T. Baron, C. Jin, I. Ross, A. Seeds and H. Liu, Monolithically Integrated Electrically Pumped Continuous-Wave III-V Quantum Dot Light Sources on Silicon, IEEE J. Sel. Top. Quantum Electron. **23**, 1900910 (2017).
34. C. Akay, P. Parrein, and J. Rolland, Estimation of longitudinal resolution in optical coherence imaging, Appl. Opt. **41**, 5256 (2002).
35. K. Nishi, K. Takemasa, and M. Sugawara, Development of Quantum Dot Lasers for Data-Com and Silicon Photonics Applications IEEE J. Sel. Topics Quantum Electronics **23**, 1901007. (2017).
36. M. Sugawara and M. Usami, Handling the heat, Nat. Photonics **3**, 30 (2009).
37. L. Li, M. Rossetti, A. Fiore, L. Occhi, and C. Velez, Wide emission spectrum from superluminescent diodes with chirped quantum dot multilayer, Electron. Lett. **41**, 41 (2005).
38. K. Zhou, Q. Jiang, Z. Zhang, S. Chen, H. Liu, Z. Lu, K. Kennedy, S. Matcher, R. Hogg, Quantum dot selective area intermixing for broadband light sources, Opt. Express, **20**, 26950 (2012).
39. S. Chen, K. Zhou, Z. Zhang, D. T. D. Childs, M. Hugues, A. J. Ramsay, and R. A. Hogg, Ultra-broad spontaneous emission and modal gain spectrum from a hybrid quantum well/quantum dot laser structure, Appl. Phys. Lett. **100**, 041118 (2012).